

**OPTIMIZATION OF 3D RECONSTRUCTION
SURFACE RENDERING ALGORITHM FOR
OSFERION BONE VOID FILLING**

DANIEL CHIN JIE YUAN

UNIVERSITI SAINS MALAYSIA

2023

**OPTIMIZATION OF 3D RECONSTRUCTION
SURFACE RENDERING ALGORITHM FOR
OSFERION BONE VOID FILLING**

by

DANIEL CHIN JIE YUAN

**Thesis submitted in fulfilment of the requirements
for the degree of
Master of Science**

September 2023

ACKNOWLEDGEMENT

Firstly, I would like to express my gratitude to the Institute of Postgraduate Studies, Universiti Sains Malaysia, and the School of Computer Sciences, Universiti Sains Malaysia, for allowing me to further my studies in the Master of Science (Computer Science) research mode. Secondly, I would like to thank my supervisor, Assoc. Prof. Dr. Ahmad Sufril Azlan Mohamed, and my co-supervisor, Assoc. Prof. Dr. Khairul Anuar Shariff, for their excellent guidance throughout the research. This masterpiece is only possible with their marvellous supervision. Thirdly, I would like to thank my panels, Assoc. Prof. Mohd Azam Osman, Prof. Dr. Riza Sulaiman, and Assoc. Prof. Dr. Wan Mohd Nazmee Wan Zainon, for their valuable feedback on improving the writing of this work. Fourthly, I would like to thank the Dean of the School of Computer Sciences, Prof. Dato' Dr. Bahari Belaton, for his time and helpful feedback on further improving the composition of this work. I would also like to thank my parents for their emotional support whenever I struggle to balance work and research well. Lastly, I thank my friends and colleagues for their suggestions for improving the research.

TABLE OF CONTENTS

ACKNOWLEDGEMENT	ii
TABLE OF CONTENTS	iii
LIST OF TABLES	viii
LIST OF FIGURES	ix
LIST OF SYMBOLS	xvii
LIST OF ABBREVIATIONS	xviii
ABSTRAK	xix
ABSTRACT	xx
CHAPTER 1 INTRODUCTION	1
1.1 Chapter Overview	1
1.2 Background	1
1.2.1 Surface Rendering	5
1.2.2 3D Imaging Techniques	5
1.2.3 OSferion Bone Void Filling	6
1.3 Research Problem.....	7
1.4 Research Questions	9
1.5 Research Objective.....	10
1.6 Research Scope and Limitations	10
1.7 Research Impact	11
1.7.1 Contribution to Knowledge.....	11
1.8 Summary	12
CHAPTER 2 LITERATURE REVIEW	13
2.1 Chapter Overview	13
2.2 3D Reconstruction.....	14
2.3 OSferion Bone Void Filling	15

2.4	Surface Rendering	16
2.4.1	Marching Cubes	17
2.4.2	Marching Tetrahedra	26
2.5	Mesh Simplification	32
2.6	Surface Smoothing	35
2.7	3D Reconstruction Optimization.....	38
2.8	Summary	41
CHAPTER 3 METHODOLOGY.....		47
3.1	Chapter Overview	47
3.2	Overview of the Research Methodology.....	47
3.3	Surface Rendering Improvement Method	49
3.4	Image Datasets	50
3.4.1	Bone Defects	51
3.5	Image Pre-processing	51
3.6	Parameter Optimization.....	54
3.6.1	3D Smoothing	55
3.6.2	Mesh Simplification	56
3.7	Most Optimal Parameter Combination Selection.....	56
3.8	3D Reconstruction.....	58
3.9	Export 3D Model.....	58
3.10	Surface Mesh Improvement Methodology.....	58
3.10.1	Surface Smoothing	59
3.11	Evaluation Metrics	60
3.11.1	RMSE.....	60
3.11.2	SSIM.....	61
3.11.3	MS-SSIM	62
3.11.4	Number of Vertices and Faces	63

3.11.5	Reconstruction Time	64
3.11.6	Rendering Time.....	64
3.12	Proposed Improvement Method vs Literature Review.....	64
3.13	Summary	66
CHAPTER 4 RESULTS AND DISCUSSION.....		67
4.1	Chapter Overview	67
4.2	Marching Cubes vs Marching Tetrahedra.....	67
4.3	Improvement and Optimization Study	70
4.4	Effect of Smoothing Kernel Type and Size on Reconstruction Accuracy	72
4.4.1	Effect of Smoothing Kernel Type and Size on RMSE.....	72
4.4.2	Effect of Smoothing Kernel Type and Size on SSIM	76
4.4.3	Effect of Smoothing Kernel Type and Size on MS-SSIM.....	78
4.5	Effect of Smoothing Kernel Type and Size on Number of Vertices and Faces	80
4.5.1	Effect of Smoothing Kernel Type and Size on Number of Vertices.....	81
4.5.2	Effect of Smoothing Kernel Type and Size on Number of Faces	83
4.6	Effect of Smoothing Kernel Type and Size on Speed.....	86
4.6.1	Effect of Smoothing Kernel Type and Size on Reconstruction Time	86
4.6.2	Effect of Smoothing Kernel Type and Size on Rendering Time	90
4.7	Effect of Gaussian Kernel Standard Deviation on Reconstruction Accuracy	92
4.7.1	Effect of Gaussian Kernel Standard Deviation on RMSE	92
4.7.2	Effect of Gaussian Kernel Standard Deviation on SSIM.....	95
4.7.3	Effect of Gaussian Kernel Standard Deviation on MS-SSIM.....	97
4.8	Effect of Gaussian Kernel Standard Deviation on Number of Vertices and Faces.....	99

4.8.1	Effect of Gaussian Kernel Standard Deviation on Number of Vertices.....	99
4.8.2	Effect of Gaussian Kernel Standard Deviation on Number of Faces.....	101
4.9	Effect of Gaussian Kernel Standard Deviation on Speed	103
4.9.1	Effect of Gaussian Kernel Standard Deviation on Reconstruction Time	103
4.9.2	Effect of Gaussian Kernel Standard Deviation on Rendering Time	106
4.10	Effect of Reduction Factor on Reconstruction Accuracy.....	108
4.10.1	Effect of Reduction Factor on RMSE	108
4.10.2	Effect of Reduction Factor on SSIM.....	111
4.10.3	Effect of Reduction Factor on MS-SSIM.....	112
4.11	Effect of Reduction Factor on Number of Vertices and Faces	114
4.11.1	Effect of Reduction Factor on Number of Vertices	114
4.11.2	Effect of Reduction Factor on Number of Faces.....	116
4.12	Effect of Reduction Factor on Speed	118
4.12.1	Effect of Reduction Factor on Reconstruction Time	118
4.12.2	Effect of Reduction Factor on Rendering Time.....	120
4.13	Improved Marching Cubes without Surface Smoothing vs with Surface Smoothing	122
4.14	Proposed Improvement Method vs Literature Review.....	125
4.14.1	Reconstruction Accuracy Comparison.....	127
4.14.2	Number of Vertices and Faces Comparison.....	132
4.14.3	Speed Comparison.....	135
4.15	Summary	139
CHAPTER 5 CONCLUSION AND FUTURE RECOMMENDATIONS....		143
5.1	Chapter Overview	143
5.2	Conclusion.....	143

5.3	Recommendations for Future Research	145
	REFERENCES.....	146
	APPENDICES	
	LIST OF PUBLICATIONS	

LIST OF TABLES

	Page
Table 2.1	Evolution of the Marching Cubes41
Table 2.2	Evolution of the Marching Tetrahedra.....42
Table 2.3	Evolution of Mesh Simplification.....44
Table 2.4	Evolution of Surface Smoothing.....45
Table 2.5	Evolution of 3D Optimization.....46
Table 4.1	Reconstruction accuracy of the Marching Cubes and the Marching Tetrahedra algorithm.....68
Table 4.2	Top three highest parameter combination score for all three image datasets70
Table 4.3	Proposed improvement method without surface smoothing vs with surface smoothing vs literature review 123

LIST OF FIGURES

	Page
Figure 1.1	Overview of single view image 3D reconstruction..... 1
Figure 1.2	Overview of multiple view image 3D reconstruction2
Figure 1.3	Overview of multiple cross-sectional images 3D reconstruction3
Figure 1.4	Surface rendering (left) and volume rendering (right) of skull (Schunke et al., 2012).....4
Figure 1.5	2D micro-CT rabbit femur image slice5
Figure 1.6	Huge number of triangle patches for Marching Cubes7
Figure 2.1	Overview of literature review organization 13
Figure 2.2	Staircase surface of surface rendering reconstructed 3D model 17
Figure 2.3	Marching Cubes between two surfaces (Lorensen & Cline, 1987) ... 18
Figure 2.4	15 unique patterns of cube triangulation (Lorensen & Cline, 1987)... 18
Figure 2.5	Marching Cubes ambiguity issue 19
Figure 2.6	33 cube configurations (Custodio et al., 2019)22
Figure 2.7	21 cube configurations (Masala et al., 2013)24
Figure 2.8	24 cube configurations (M. N. Wang et al., 2020).....25
Figure 2.9	Different tetrahedra orientations (Bourke, 1994).....26
Figure 2.10	Tetrahedra configurations (Bourke, 1994).....27
Figure 2.11	Edge-cuts classification (Bagley et al., 2016).....29
Figure 2.12	C3D10 element edge intersections (Ren et al., 2021).....31
Figure 3.1	Overall methodology.....48
Figure 3.2	Proposed improvement method.....49
Figure 3.3	Sample micro-CT images for all three datasets50
Figure 3.4	Image pre-processing steps51

Figure 3.5	Results of different edge detection method on image dataset 1.....	53
Figure 3.6	Most optimal parameter combination selection workflow	57
Figure 3.7	Proposed improvement method with surface smoothing.....	59
Figure 3.8	Proposed improvement vs traditional surface rendering algorithms	60
Figure 3.9	Overall workflow of proposed improvement vs literature review	65
Figure 4.1	Close up view of the reconstructed 3D models with the Marching Cubes versus the Marching Tetrahedra.....	69
Figure 4.2	Reconstructed 3D models with the proposed improvement method	71
Figure 4.3	Close up view of the 3D models for box versus Gaussian.....	73
Figure 4.4	Bar chart of RMSE against smoothing kernel type and size for Image Dataset 1.....	73
Figure 4.5	Bar chart of RMSE against smoothing kernel type and size for Image Dataset 2.....	74
Figure 4.6	Bar chart of RMSE against smoothing kernel type and size for Dataset 3.....	75
Figure 4.7	Close up view of the 3D models for different smoothing kernel sizes	75
Figure 4.8	Bar chart of SSIM against smoothing kernel type and size for Image Dataset 1	76
Figure 4.9	Bar chart of SSIM against smoothing kernel type and size for Image Dataset 2.....	77
Figure 4.10	Bar chart of SSIM against smoothing kernel type and size for Image Dataset 3.....	77
Figure 4.11	Bar chart of MS-SSIM against smoothing kernel type and size for Image Dataset 1	79
Figure 4.12	Bar chart of MS-SSIM against smoothing kernel type and size for Image Dataset 2.....	79

Figure 4.13	Bar chart of MS-SSIM against smoothing kernel type and size for Image Dataset 3.....	80
Figure 4.14	Bar chart of vertices against smoothing kernel type and size for Image Dataset 1.....	81
Figure 4.15	Bar chart of vertices against smoothing kernel type and size for Image Dataset 2.....	82
Figure 4.16	Bar chart of vertices against smoothing kernel type and size for Image Dataset 3.....	82
Figure 4.17	Bar chart of faces against smoothing kernel type and size for Image Dataset 1.....	84
Figure 4.18	Bar chart of faces against smoothing kernel type and size for Image Dataset 2.....	85
Figure 4.19	Bar chart of faces against smoothing kernel type and size for Image Dataset 3.....	85
Figure 4.20	Bar chart of reconstruction time against smoothing kernel type and size for Image Dataset 1.....	86
Figure 4.21	Bar chart of reconstruction time against smoothing kernel type and size for Image Dataset 2.....	87
Figure 4.22	Bar chart of reconstruction time against smoothing kernel type and size for Image Dataset 3.....	88
Figure 4.23	Bar chart of rendering time against smoothing kernel type and size for Image Dataset 1.....	90
Figure 4.24	Bar chart of rendering time against smoothing kernel type and size for Image Dataset 2.....	91
Figure 4.25	Bar chart of rendering time against smoothing kernel type and size for Image Dataset 3.....	91
Figure 4.26	Bar chart of RMSE against Gaussian standard deviation for Image Dataset 1.....	93
Figure 4.27	Bar chart of RMSE against Gaussian standard deviation for Image Dataset 2.....	93

Figure 4.28	Bar chart of RMSE against Gaussian standard deviation for Image Dataset 3.....	94
Figure 4.29	Close up view of the 3D models with different standard deviation...	95
Figure 4.30	Bar chart of SSIM against Gaussian standard deviation for Image Dataset 1.....	96
Figure 4.31	Bar chart of SSIM against Gaussian standard deviation for Image Dataset 2.....	96
Figure 4.32	Bar chart of SSIM against Gaussian standard deviation for Image Dataset 3.....	97
Figure 4.33	Bar chart of MS-SSIM against Gaussian standard deviation for Image Dataset 1.....	98
Figure 4.34	Bar chart of MS-SSIM against Gaussian standard deviation for Image Dataset 2.....	98
Figure 4.35	Bar chart of MS-SSIM against Gaussian standard deviation for Image Dataset 3.....	99
Figure 4.36	Bar chart of vertices against Gaussian standard deviation for Image Dataset 1.....	100
Figure 4.37	Bar chart of vertices against Gaussian standard deviation for Image Dataset 2.....	100
Figure 4.38	Bar chart of vertices against Gaussian standard deviation for Image Dataset 3.....	101
Figure 4.39	Bar chart of faces against Gaussian standard deviation for Image Dataset 1.....	102
Figure 4.40	Bar chart of faces against Gaussian standard deviation for Image Dataset 2.....	102
Figure 4.41	Bar chart of faces against Gaussian standard deviation for Image Dataset 3.....	103
Figure 4.42	Bar chart of reconstruction time against Gaussian standard deviation for Image Dataset 1.....	104

Figure 4.43	Bar chart of reconstruction time against Gaussian standard deviation for Image Dataset 2	104
Figure 4.44	Bar chart of reconstruction time against Gaussian standard deviation for Image Dataset 3	105
Figure 4.45	Bar chart of rendering time against Gaussian standard deviation for Image Dataset 1	106
Figure 4.46	Bar chart of rendering time against Gaussian standard deviation for Image Dataset 2	107
Figure 4.47	Bar chart of rendering time against Gaussian standard deviation for Image Dataset 3	107
Figure 4.48	Bar chart of RMSE against mesh simplification reduction factor for Image Dataset 1	108
Figure 4.49	Bar chart of RMSE against mesh simplification reduction factor for Image Dataset 2	109
Figure 4.50	Bar chart of RMSE against mesh simplification reduction factor for Image Dataset 3	109
Figure 4.51	Close up view of 3D models with different reduction factors	110
Figure 4.52	Bar chart of SSIM against mesh simplification reduction factor for Image Dataset 1	111
Figure 4.53	Bar chart of SSIM against mesh simplification reduction factor for Image Dataset 2	111
Figure 4.54	Bar chart of SSIM against mesh simplification reduction factor for Image Dataset 3	112
Figure 4.55	Bar chart of MS-SSIM against mesh simplification reduction factor for Image Dataset 1	112
Figure 4.56	Bar chart of MS-SSIM against mesh simplification reduction factor for Image Dataset 2	113
Figure 4.57	Bar chart of MS-SSIM against mesh simplification reduction factor for Image Dataset 3	113

Figure 4.58	Bar chart of vertices against mesh simplification reduction factor for Image Dataset 1	114
Figure 4.59	Bar chart of vertices against mesh simplification reduction factor for Image Dataset 2	115
Figure 4.60	Bar chart of vertices against mesh simplification reduction factor for Image Dataset 3	115
Figure 4.61	Bar chart of faces against mesh simplification reduction factor for Image Dataset 1	116
Figure 4.62	Bar chart of faces against mesh simplification reduction factor for Image Dataset 2.....	117
Figure 4.63	Bar chart of faces against mesh simplification reduction factor for Image Dataset 3.....	117
Figure 4.64	Bar chart of reconstruction time against mesh simplification reduction factor for Image Dataset 1.....	118
Figure 4.65	Bar chart of reconstruction time against mesh simplification reduction factor for Image Dataset 2.....	119
Figure 4.66	Bar chart of reconstruction time against mesh simplification reduction factor for Image Dataset 3.....	119
Figure 4.67	Bar chart of rendering time against mesh simplification reduction factor for Image Dataset 1.....	120
Figure 4.68	Bar chart of rendering time against mesh simplification reduction factor for Image Dataset 2.....	121
Figure 4.69	Bar chart of rendering time against mesh simplification reduction factor for Image Dataset 3.....	121
Figure 4.70	Close up view of 3D models without smoothing vs with smoothing	124
Figure 4.71	Close up view of the reconstructed 3D models using the proposed improvement method vs the literature review.....	126
Figure 4.72	Proposed improvement method vs literature review.....	127

Figure 4.73	Bar chart of RMSE against improved Marching Cubes methods for Image Dataset 1	127
Figure 4.74	Bar chart of RMSE against improved Marching Cubes methods for Image Dataset 2.....	128
Figure 4.75	Bar chart of RMSE against improved Marching Cubes methods for Image Dataset 3.....	128
Figure 4.76	Bar chart of SSIM against improved Marching Cubes methods for Image Dataset 1	129
Figure 4.77	Bar chart of SSIM against improved Marching Cubes methods for Image Dataset 2.....	129
Figure 4.78	Bar chart of SSIM against improved Marching Cubes methods for Image Dataset 3.....	130
Figure 4.79	Bar chart of MS-SSIM against improved Marching Cubes methods for Image Dataset 1	130
Figure 4.80	Bar chart of MS-SSIM against improved Marching Cubes methods for Image Dataset 2	131
Figure 4.81	Bar chart of MS-SSIM against improved Marching Cubes methods for Image Dataset 3	131
Figure 4.82	Bar chart of vertices and faces against improved Marching Cubes methods for Image Dataset 1.....	133
Figure 4.83	Bar chart of vertices and faces against improved Marching Cubes methods for Image Dataset 2.....	133
Figure 4.84	Bar chart of vertices and faces against improved Marching Cubes methods for Image Dataset 3.....	134
Figure 4.85	Bar chart of reconstruction time against improved Marching Cubes methods for Image Dataset 1.....	135
Figure 4.86	Bar chart of reconstruction time against improved Marching Cubes methods for Image Dataset 2.....	136
Figure 4.87	Bar chart of reconstruction time against improved Marching Cubes methods for Image Dataset 3.....	136

Figure 4.88	Bar chart of rendering time against improved Marching Cubes methods for Image Dataset 1.....	137
Figure 4.89	Bar chart of rendering time against improved Marching Cubes methods for Image Dataset 2.....	137
Figure 4.90	Bar chart of rendering time against improved Marching Cubes methods for Image Dataset 3.....	138

LIST OF SYMBOLS

M	Number of pixels in the image
i	Pixel intensity value
$S(i)$	Source image
$D(i)$	Original image
μ	Local mean
C	Weak denominators
σ^2	Variance
σ_{SD}	Covariance of S and D
α, β, γ	Weights
P	Number of down samplings to reduce the image resolution
j	Original image resolution

LIST OF ABBREVIATIONS

3D	Three-dimensional
2D	Two-dimensional
MVS	Multi-View Stereo
MDN	Multi-View Deformation Network
CT	Computed Tomography
MRI	Magnetic Resonance Imaging
Micro-CT	Micro-computed Tomography
CBCT	Cone Beam Computed Tomography
DPI	Dots Per Inch
GB	Gigabytes
GPU	Graphics Processing Unit
FOV	Field of View
LiDAR	Light Detection and Ranging technique
SEM	Scanning Electron Microscope
SBF-SEM	Serial Block Face Scanning Electron Microscope
AF	Annulus Fibrosus
IVD	Intervertebral Disc
DTI	Diffusion Tensor Imaging
ROI	Region of Interest
HC	Humphrey's Classes
DCRS	Delayed Controlled Random Search
EGEE	European Grid for E-ScienE program
CRS	Controlled Random Search
RASL	Robust Alignment by Sparse and Low-rank decomposition
SQP	Sequential Quadratic Programming
PALM	Parameter-adjusting Levenberg-Marquardt
STL	Standard Tessellation Language
RGB	Red Green Blue
RMSE	Root Mean Squared Error
SSIM	Structural Similarity Index
MS-SSIM	Multiscale Structural Similarity Index

PENGOPTIMUMAN ALGORITMA PENJANAAN PERMUKAAN REKONSTRUKSI 3D UNTUK PENGISIAN RONGGA TULANG OSFERION

ABSTRAK

Rekonstruksi 3D merupakan proses pemodelan model 3D daripada imej 2D. Proses ini terbukti berguna kepada doktor dan pakar bedah dalam proses diagnosis dan perancangan pembedahan untuk rongga tulang OSferion yang terkenal dengan kadar penyerapannya yang pantas. Antara kaedah rekonstruksi 3D, kaedah rekonstruksi penjanaan permukaan lebih sesuai dalam menggambarkan struktur dan bentuk tulang. Walau bagaimanapun, kaedah rekonstruksi penjanaan permukaan mempunyai dua masalah utama, iaitu model 3D mempunyai bilangan yang besar bagi tompok segi tiga, dan proses yang perlahan, terutamanya dataset 2D yang lebih besar. Selain itu, permukaan model mudah terjejas semasa proses mengecilkan saiz fail untuk meningkatkan kemudahan model 3D. Oleh yang demikian, objektif penyelidikan ini adalah untuk menambahbaik algoritma Marching Cubes atau Marching Tetrahedra daripada imej CT/MRI yang besar, dan meningkatkan kualiti permukaan model 3D selepas proses pengurangan tompok segi tiga. Faedah yang boleh diperolehi daripada kajian ini termasuk penambahbaikan kemudahan model 3D agar doktor dan pakar bedah mempunyai akses kepada model 3D pada bila-bila masa dan di mana-mana sahaja. Kaedah perbaikan yang dicadangkan, iaitu Marching Cubes dengan pemulasan data 3D saiz kotak 11, faktor pengurangan 0.1, dan permukaan pemulasan 3D saiz kotak 11, berjaya meningkatkan ketepatan rekonstruksi sebanyak 6.26%, mengurangkan bilangan tompok segi tiga sebanyak 89.82%, dan mengurangkan masa rekonstruksi sebanyak 52.45% saat dan masa pemaparan sebanyak 90.74% saat.

OPTIMIZATION OF 3D RECONSTRUCTION SURFACE RENDERING ALGORITHM FOR OSFERION BONE VOID FILLING

ABSTRACT

3D reconstruction visualizes the 3D models from 2D medical image slices, which is proven helpful to doctors and surgeons in diagnosing and surgical planning on OSferion bone defects, which is well known for its fast absorption rate. Among the 3D reconstruction algorithms, surface rendering algorithms are more suitable for effectively visualizing the bones' structure and shape. However, surface rendering algorithms have two main problems, the massive number of triangular patches generated during the reconstruction process and the slow reconstruction speed, especially in reconstructing huge medical image datasets. Also, with the attempt to generate rendering-device-agnostic models by reducing the 3D models' file size, the surface of the models is easily deformed due to the reduced number of triangular patches. Thus, the objectives are to enhance the Marching Cubes or the Marching Tetrahedra algorithm for large CT/MRI datasets so that the reconstructed 3D models are rendering-device-agnostic and optimized and to improve the quality of the 3D models after reducing the number of vertices and faces so that the surface of the 3D models can be improved. The impact of this research includes 3D models that are rendering-device-agnostic so that doctors and surgeons have access to the 3D models at anytime, anywhere. The proposed improvement method, which is Marching Cubes with 3D data smoothing and surface smoothing box kernel size of 11, mesh decimation reduction factor of 0.1, successfully increased the reconstruction accuracy by 6.26%, decreased the number of vertices and faces by 89.82%, and decreased the reconstruction and rendering time by 52.45% and 90.74% seconds respectively.

CHAPTER 1

INTRODUCTION

1.1 Chapter Overview

This chapter introduces the research that focuses on optimizing the 3D reconstruction surface rendering algorithm for OSferion bone void filling. In Chapter 1.2, the background of surface rendering, 3D imaging techniques, and OSferion bone void filling are presented. The research problem, research questions, and research objectives are addressed by the following sections, 1.3, 1.4, and 1.5, respectively. Chapter 1.6 defines the scope and limitations of this study, while Chapter 1.7 highlights the research's impact and contribution to the body of knowledge. Finally, Chapter 1.8 provides a summary of the key points discussed in this chapter.

1.2 Background

Three-dimensional (3D) reconstruction is the process of converting two-dimensional (2D) image(s) into its equivalent 3D form. It allows the 3D profile of the object to be captured and visualized in a 3D space. The input of this process can be one single-view 2D image, multiple-view 2D images, or a set of 2D images.

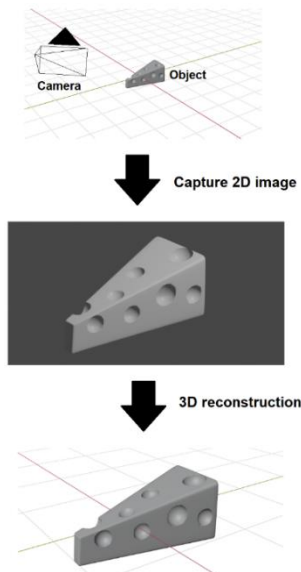


Figure 1.1 Overview of single view image 3D reconstruction

Single-view image 3D reconstruction, as the name implies, uses a single-view image as input and attempts to output its equivalent 3D object (Thai et al., 2021). As shown in Figure 1.1, a single 2D image is captured with a camera at an angle with sufficient depth information and then reconstructed into a 3D model. This method relies heavily on the captured image's quality and the angle at which the object is captured for accurate reconstruction. Also, this method is unreliable for reconstructing complex objects as there is not enough information on the other side of the object from the captured angle (Thai et al., 2021). This method is only suitable for reconstructing the object's surface as the underlying surface cannot be captured through the camera. An example of this reconstruction technique is point cloud reconstruction (Ping et al., 2022).

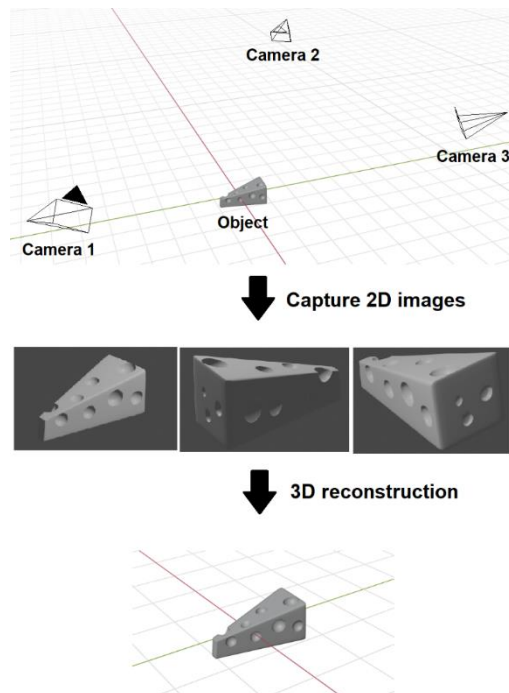


Figure 1.2 Overview of multiple view image 3D reconstruction

Multiple-view image 3D reconstruction, on the other hand, inputs multiple 2D images captured at different angles and outputs its equivalent 3D object (Hu et al., 2021). As shown in Figure 1.2, three 2D images are captured with adequate depth information at different angles before being reconstructed into a 3D model. Although

more images are used during the reconstruction process, it is generally more reliable than single-view image 3D reconstruction as more information on the object can be obtained, making the reconstructed 3D model more accurate. However, this method still relies heavily on the captured images' quality and the angle at which the object is captured for accurate reconstruction. Like single-view image 3D reconstruction, this method is only suitable for reconstructing the object's surface as the underlying surface cannot be captured through the camera. Examples of this method include Multi-View Stereo (MVS) and Multi-View Deformation Network (MDN) (Wen et al., 2019).

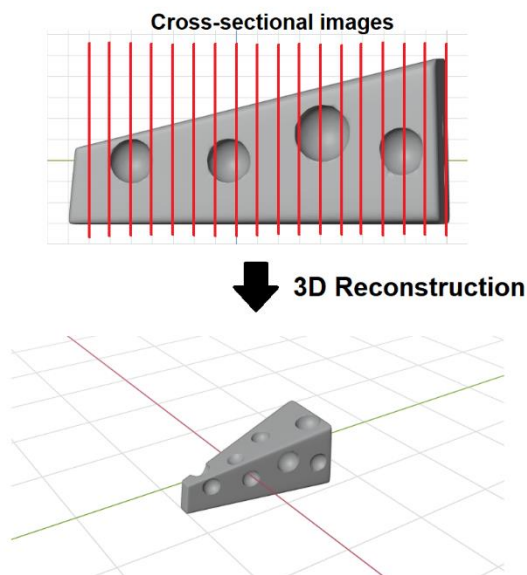


Figure 1.3 Overview of multiple cross-sectional images 3D reconstruction

Multiple image 3D reconstruction in the medical field inputs a set of cross-sectional 2D images generated from 3D medical imaging technologies like Computed Tomography (CT) and Magnetic Resonance Imaging (MRI) scan and outputs a 3D model (Jehn et al., 2020; Jie et al., 2020; Kang et al., 2020). According to Figure 1.3, the object is first scanned with a 3D medical imaging scanner like a CT and MRI scan, which outputs an image stack of the object's cross-sectional slices. These cross-sectional slices are then stacked and then reconstructed into a 3D model. Although the image quality of the image slices is still essential as there may be artifacts in the

images, this method is generally more reliable than the other two methods as depth information is not required to reconstruct into a 3D model accurately. Besides that, the underlying surface can also be visualized since the images are captured as cross-sectional slices rather than just the surface. Examples of methods in this category are surface and volume rendering techniques (van Ooijen et al., 2003; Udupa et al., 1991).

In this research, multiple images 3D reconstruction is preferred over single-view and multiple-view image 3D reconstruction as it is often applied in the medical field for visualizing medical images as 3D models. Besides that, it is generally more reliable than single-view and multiple-view 3D reconstruction in reconstructing human or animal body parts.

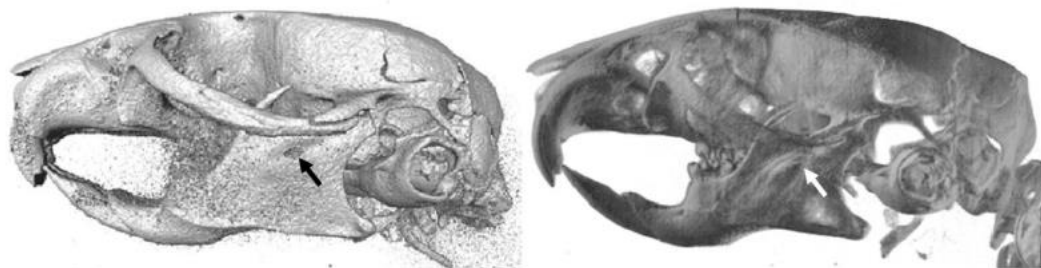


Figure 1.4 Surface rendering (left) and volume rendering (right) of skull (Schunke et al., 2012)

Both surface rendering and volume rendering techniques have their own merits and demerits. Based on Figure 1.4, surface rendering techniques help visualize the structure and shape of human or animal body parts, whereas volume rendering techniques are useful in visualizing human or animal internal structures and organs. As this research mainly focuses on visualizing and studying the bones' structure and shape, surface rendering is selected over volume rendering.

1.2.1 Surface Rendering

Surface rendering is a subdomain of multiple images 3D reconstruction that visualizes medical images as isosurfaces formed through triangulation of vertices and faces. Surface rendering is more suitable for visualizing body parts with definite structures and shapes like bones than volume rendering.

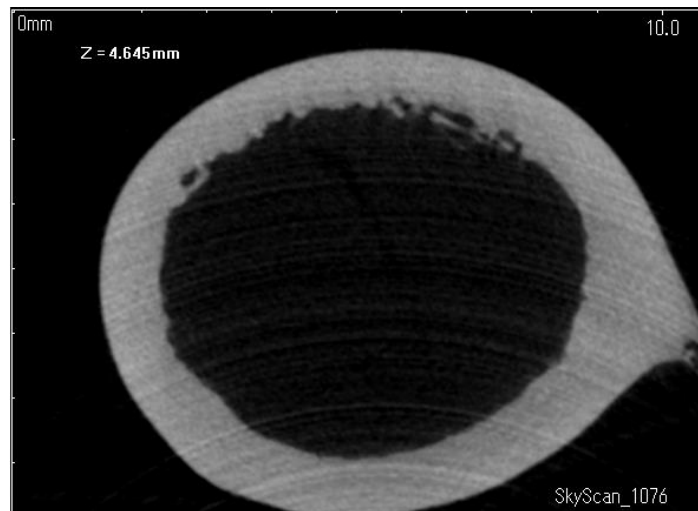


Figure 1.5 2D micro-CT rabbit femur image slice

Surface rendering techniques are applied over 2D micro-computed tomography (micro-CT) bone defect image slices to visualize and study the bones' structure and shape. Figure 1.5 illustrates a sample image slice of the bone defect.

1.2.2 3D Imaging Techniques

3D imaging techniques are essential for doctors and surgeons to diagnose diseases and monitor the treatment progress. It also allows the diagnosis and surgical planning process to occur without damaging the bone defect. With the advancement of technologies, various 3D imaging techniques with different advantages, disadvantages, and applications have been discovered (Karatas & Toy, 2014). Examples of 3D imaging techniques are CT, MRI, Cone Beam Computed Tomography (CBCT), and micro-CT.

Although CT scan remains very popular in recent studies related to bone and 3D visualization (Ahmad et al., 2020; Hao et al., 2020; Alp et al., 2020; Raiss et al., 2020; Rollo et al., 2021), micro-CT is also a popular choice (Huang et al., 2020; Jandl et al., 2020). Micro-CT imaging is preferred over CT imaging when the sample size is small, and images of higher resolution are needed to aid the evaluation process. Besides that, micro-CT imaging is relatively inexpensive compared to other medical imaging techniques like MRI. However, micro-CT images are also easily susceptible to noises like ring artifacts.

Due to the poor clarity of the micro-CT images, 3D reconstruction techniques become essential for doctors and surgeons. With the 3D reconstructed bone defect models, doctors and surgeons can view and analyze the bone defects with great accuracy (Alasal et al., 2021; Al-Mnayyis et al., 2020). This advantage prevents doctors and surgeons from making wrong judgments during diagnosis and surgical planning.

1.2.3 OSferion Bone Void Filling

Bone defects are a form of bone deficiency whereby the bones are not complete. Various factors like cancer, trauma, and infection can cause them. One of the most common bone defects is bone voids. Typical treatment for bone voids includes bioceramic fillers and bone grafts. Although bone grafts offer excellent stability, they are limited in supply and may lead to complications; hence bioceramic fillers may be preferred over bone grafting. There are many bioceramic fillers available in the medical field. One of the popular fillers is OSferion.

In this research, the micro-CT image stacks used are bone voids filled with a bone void filler called OSferion (Bulgin & Hodzic, 2017). OSferion enables the replacement and resorption of bone during the healing process of bone damage. A

ceramic material (Mohammadi et al., 2019) is applied to the bone defect area, and the OSferion structure is captured using an in vivo micro-CT scanner called SkyScan. The result of the scan is an array of 2D bone defect image slices.

1.3 Research Problem

The Marching Cubes and the Marching Tetrahedra algorithms, which are among the most popular algorithms for performing surface rendering, have two main issues: a massive number of triangle patches referring to Figure 1.6 and a long reconstruction time. These two issues will become a bigger problem when the image slices' dimensions to be reconstructed are huge.

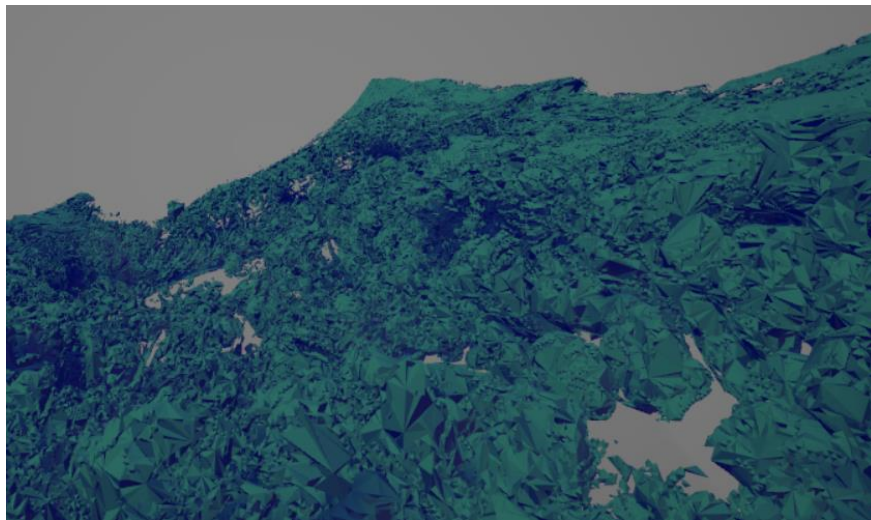


Figure 1.6 Huge number of triangle patches for Marching Cubes

Even though many approaches were taken to solve the issues (Chen et al., 2021; Gu et al., 2021; Tobin et al., 2021; Alldieck et al., 2018), these improvements are tested with image datasets with every image dimension between 300-500 pixels by 300-500 pixels by 100-500 image slices. This raises a question on the reliability of the improvements in reconstructing image datasets with their individual image dimension over 500 pixels horizontally and vertically, and over 500 image slices, into their respective 3D models. Also, the 3D models reconstructed with such image datasets

may or may not be rendering-device-agnostic, which questions the practicality of the improvements in the real world whereby not all doctors and surgeons have access to higher-end spec rendering devices like servers with 32 gigabytes (GB) memory and better graphics processing unit (GPU) like NVIDIA Quadro series, which are necessary specifications to run 3D rendering at high speed and rendering quality.

Information on the size of the image datasets used for reconstruction is vital as the number of image slices and dimensions directly impact the size of the 3D model. The size of the 3D model will determine whether the 3D model can be viewed using lower-end spec rendering devices like older models of smartphones and tablets having 4GB memory. As not all surgeons and doctors have access to higher-end spec rendering devices all the time and not all the medical image stacks are low in size, it is important to identify methods in reducing the triangular patches and reconstruction speed, especially for image datasets with individual images having over 500 pixels horizontally and vertically and over 500 image slices. Besides that, it is crucial to guarantee that the 3D models are rendering-device-agnostic so that doctors and surgeons that do not have access to higher-end spec rendering devices can also visualize the 3D models at any given time and place.

Also, the model's shape will be compromised when reducing the number of triangular patches, resulting in reduced clarity and originality of the 3D model. When the number of vertices and faces are reduced, the number of triangular patches representing the isosurface will also decrease. When the shape and originality of the 3D models are affected, the 3D models will become less accurate in representing the actual bone defect, directly affecting the doctor's and surgeon's judgement in

analyzing the bone defect. Hence, it is also equally important to improve the surface of the 3D models so that the visualization aspect will not be affected.

To summarize, in this research, the 3D reconstruction surface rendering algorithms, namely the Marching Cubes and the Marching Tetrahedra algorithm, and the reconstructed 3D models are optimized in terms of the number of vertices and faces. This is to guarantee that the reconstructed 3D models are rendering-device-agnostic and improve the reconstruction speed to enhance the efficiency of the surface rendering algorithm for image datasets with over 500 pixels horizontally and vertically and over 500 images. Besides that, the surface of the 3D models is also optimized after reducing the number of vertices and faces to improve the visualization aspect of the 3D models.

1.4 Research Questions

In this research, two main problems are addressed. Firstly, the massive number of triangular patches and long reconstruction process of traditional surface rendering algorithms, namely the Marching Cubes and the Marching Tetrahedra algorithm, upon the successful reconstruction of medical image datasets with over 500 pixels horizontally and vertically and over 500 images impact the visualization of the reconstructed 3D models, especially for lower-end spec rendering devices. Secondly, the distorted 3D model surfaces after reducing the number of triangular patches which impacts the surface quality of the 3D models.

With that in mind, to address the mentioned issues in this research, two research questions can be formulated as such:

1. What improvements can be made to the traditional 3D reconstruction surface rendering algorithm, either the Marching Cubes or the Marching Tetrahedra algorithm, to optimize the number of vertices and faces and reconstruction speed so that the 3D models are guaranteed to be rendering-device-agnostic for image datasets with over 500 pixels horizontally and vertically and over 500 images?
2. How can the surface of the 3D models be improved after reducing the number of vertices and faces so that the surface quality of the 3D models can be enhanced?

1.5 Research Objective

To answer the research questions articulated in the previous section, two research objectives that will be targeted to achieve at the end of this research can be constructed as such:

1. To enhance the Marching Cubes or the Marching Tetrahedra algorithm for large CT/MRI datasets so that the reconstructed 3D models are rendering-device-agnostic and optimized.
2. To improve the quality of the 3D models after reducing the number of vertices and faces so that the surface of the 3D models can be improved.

1.6 Research Scope and Limitations

To achieve the research objectives, this research will only explore and improve 3D reconstruction surface rendering algorithms, either the Marching Cubes or the Marching Tetrahedra algorithm. Other reconstruction methods like volume rendering

and cinematic rendering are excluded. Besides that, this research will only optimize the number of vertices and faces, reconstruction and rendering speed, and surface of the 3D models.

This research defines a large image dataset as every image slice having over 500 pixels horizontally, vertically, and over 900 image slices. The image datasets are of animal samples and can be in any format, as the image stacks from the medical imaging devices can be in various formats with the condition that the image processing library supports them. They are contributed by Assoc. Prof. Dr. Khairul Anuar Shariff from the School of Materials and Mineral Resources Engineering, Universiti Sains Malaysia. The same computer will be used from the start of the research until the end to ensure that the results are fair and accurate.

1.7 Research Impact

By the end of this research, a refined Marching Cubes or the Marching Tetrahedra method to generate 3D models that are rendering-device-agnostic for large medical images is expected to prove that 3D models with high quality and rendering-device-agnostic are plausible. Besides that, the refined surface rendering method is also expected to generate 3D models of good quality even after reducing the model size to ameliorate the surface quality of the reconstructed bone defects.

1.7.1 Contribution to Knowledge

The main contribution of this research is a refined Marching Cubes or the Marching Tetrahedra method that is optimized in terms of speed, and the number of vertices and faces without sacrificing the reconstruction accuracy for large medical image datasets. The reconstructed 3D models through the refined surface rendering method are also rendering-device-agnostic for visualization.

Furthermore, the 3D models are improved after reducing the vertices and faces so that the surface of the 3D models is refined. Besides that, a 3D smoothing method is verified to be comparable to the conventional mesh smoothing methods.

1.8 Summary

This research will aim to achieve two objectives. One, to refine the Marching Cubes or the Marching Tetrahedra algorithm so that the 3D models are viewable in lower-end spec rendering devices. Two, to improve the quality of the 3D models after reducing the number of vertices and faces so that the surface of the 3D models can be refined. The impact of this research includes a refined Marching Cubes or the Marching Tetrahedra method that is optimized in terms of number of vertices and faces, speed, and surface quality without sacrificing the reconstruction accuracy for large image datasets. The refined surface rendering method is also expected to generate 3D models that are rendering-device agnostic.

CHAPTER 2

LITERATURE REVIEW

2.1 Chapter Overview

This chapter presents a literature review of 3D reconstruction technologies, related 3D rendering tools, and an overview of OSferion bone void filling. Chapter 2.2 presents the overview of the 3D reconstruction process, followed by a description of OSferion bone void filling in Chapter 2.3. The detailed related surface rendering algorithms are discussed in Chapters 2.3, 2.4, 2.5, and 2.6. The detailed 3D reconstruction optimization approach is elaborated in Chapter 2.7 to simplify the calculation and obtaining of a set of optimal parameter values. Finally, the summary of this chapter will be presented in Chapter 2.8. An overview of the organization of the literature review is illustrated in Figure 2.1.

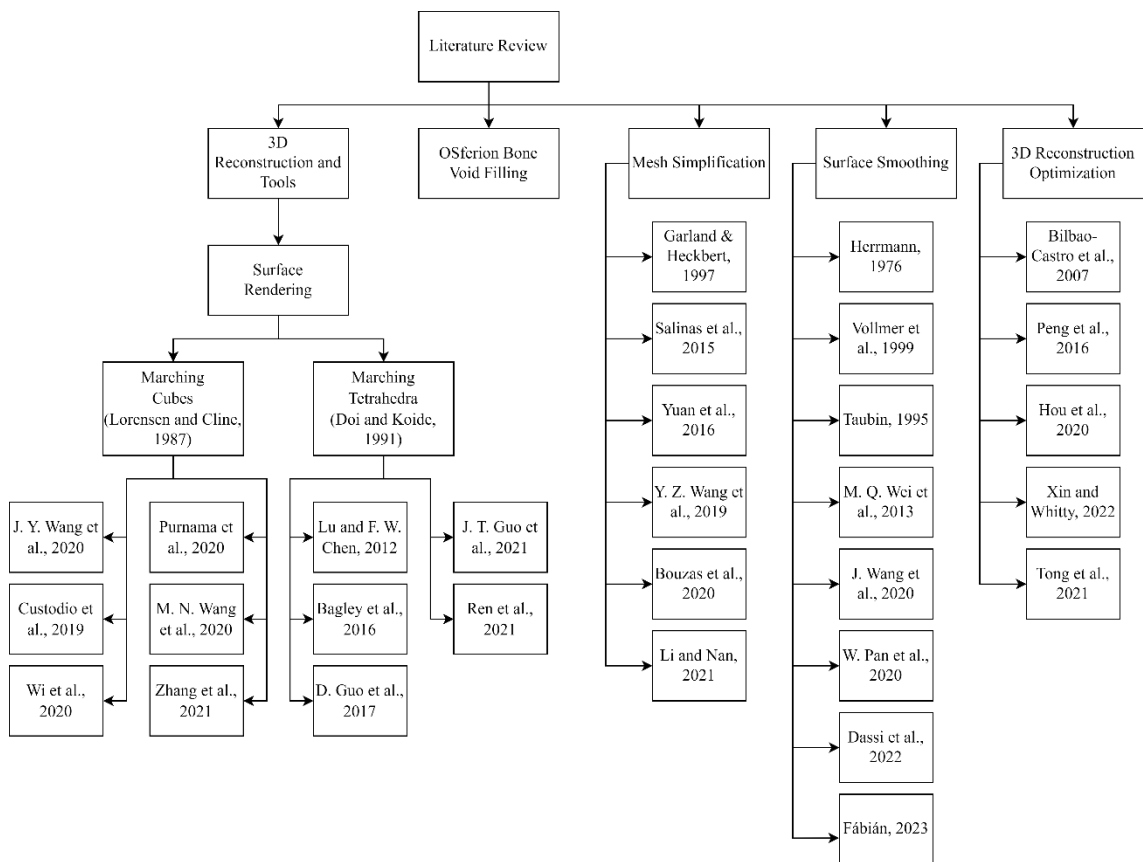


Figure 2.1 Overview of literature review organization

2.2 3D Reconstruction

3D reconstruction is a process that allows the 3D volumetric data to be captured and visualized from 2D images. 3D reconstruction is widely applied in computer vision and computer graphics. In computer vision, 3D objects were reconstructed and detected through binocular vision using two cameras, resulting in an overlapping field of view (FOV), a laser plane, and a 3D orientation board (Chen et al., 2021). Binocular vision was also used to reconstruct welding pool surfaces using two cameras with a calibration system to prevent camera distortions (Gu et al., 2021). 3D reconstruction was also applied in depth and intensity reconstruction for far-distance real-time moving scene reconstruction using the single-photon Light Detection and Ranging technique (LiDAR) (Tobin et al., 2021). In video processing, 3D reconstruction was used to build accurate 3D human models using a video consisting of human motion (Alldieck et al., 2018).

Besides that, 3D reconstruction is widely applied in various fields requiring computer vision to perform specific tasks. In archaeology, 3D reconstruction was used for digitizing historical artifacts and remains (Santos et al., 2017). 3D reconstruction was also used in visualizing complex architectures (Pepe & Constantino, 2021). 3D reconstruction was also applied in many cases of reconstructing samples scanned using a Scanning Electron Microscope (SEM) like structures of hatched larvae and young juveniles of *Oikopleura dioica* examined using Serial Block Face Scanning Electron Microscope (SBF-SEM) (Nishida et al., 2021).

In addition, 3D reconstruction is applied frequently in reconstructing animal and human body parts using medical images. For example, the annulus fibrosus (AF) in the intervertebral disc (IVD) was reconstructed, visualized, and tracked from Diffusion

Tensor Imaging (DTI) images (Stein et al., 2021). The reconstructed 3D models were also used for measurement purposes in which the measurements were helpful in surgical planning (Bao et al., 2021; Tuecking et al., 2021). The measurements also benefited virtual simulations for preoperative plans and personalized surgery (W. C. Wu et al., 2021; Bosc et al., 2021; S. L. Wang et al., 2021).

In the market, there are 3D rendering tools that offer 3D surface rendering features to visualize 3D models. Meshlab, an open-source 3D rendering tool, provides surface reconstruction features (Lindquist et al., 2021). Materialise Mimics is a paid 3D rendering tool that provides reconstruction services for medical images (Schottey et al., 2023). Thermofisher Amira is another 3D rendering tool like Materialise Mimics that offers processing and visualization methods for medical images (Arbex et al., 2022; Chickness et al., 2022). Fujifilm Synapse3D is another paid 3D rendering software for visualizing medical images (Montalti et al., 2023).

2.3 OSferion Bone Void Filling

Bone defects can be generally categorized into four types: limited defects, bone fragments have contact, bone defects have no contact, and complete articular defects (Solomin & Slongo, 2016). The categories are in increasing order of bone defect area.

Limited defects are the smallest defects among the categories where the bones are missing externally and internally on a smaller scale. One example of such a defect is bone voids. Bone fragments have contact category, which means the bones are missing on a slightly larger scale on the external part of the bone extending internally, but the bone is still connected between the top and bottom half. Bone fragments have no contact means the bones are missing on an even larger scale, including the top and bottom parts of the bone. Lastly, complete articular defects are missing bones on an

even larger scale to the point of missing either the top or bottom part of the bone, requiring more fillers and bone grafting to stabilize the bone.

Bioceramic fillers are popular for bone void treatment due to the reduced complication rate. One of the common choices for bioceramic fillers is OSferion, which is made up of 100% beta-tricalcium phosphate, offering a faster absorption rate (Bulgin & Hodzic, 2017; Noguchi et al., 2019).

2.4 Surface Rendering

Surface rendering is one of the subdomains of 3D reconstruction. Other subdomains include volume rendering and cinematic rendering, which are not discussed in this research as the focus is surface rendering. Surface rendering differs from volume rendering and cinematic rendering in that it deposits isosurface comprised of triangular patches on segmented images or region of interest (ROI) contours per image slice. The resultant 3D model is isosurfaces arranged based on the image stack.

3D models reconstructed using surface rendering algorithms benefit from the ability to visualize and analyze the surface of the models as they are made up of meshes. Surface rendering is also more suitable for visualizing structures with well-defined surfaces, like bones. Besides that, surface rendering is relatively less expensive than volume rendering and cinematic rendering, allowing better 3D model interactivity. In addition, surface rendering allows accurate 3D model measurement.

However, surface rendering algorithms generally suffer from two issues, one being a massive number of triangular patches resulting in huge 3D model sizes and two being slow reconstruction speed (J. Y. Wang et al., 2020). The issues are even more apparent in reconstructing huge image stacks. On top of that, the reconstructed 3D models often suffer from the staircase surface, as seen in Figure 2.2. Surface rendering

is also unsuitable for reconstructing and visualizing structures with ambiguous surfaces, like organs and tissues. Besides that, surface rendering cannot reconstruct and visualize internal structures if there is an external structure, like visualizing a human or animal external body with internal organs and tissues simultaneously. In both cases, volume rendering and cinematic rendering are more suitable.

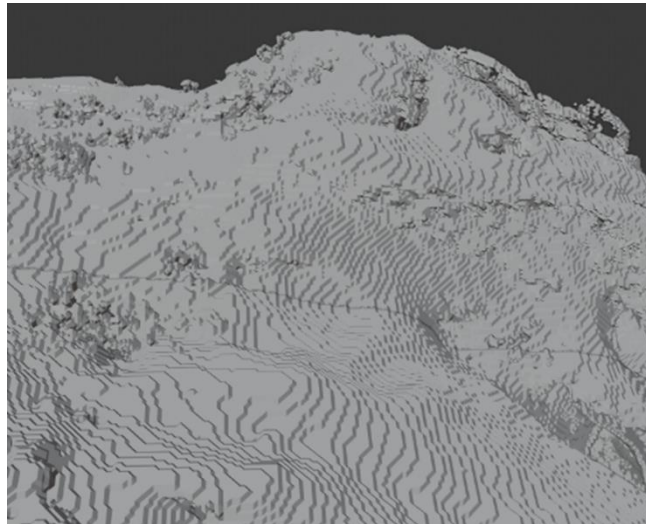


Figure 2.2 Staircase surface of surface rendering reconstructed 3D model

In this research, the two most popular surface rendering algorithms are discussed: the Marching Cubes algorithm and Marching Tetrahedra algorithm. Marching Tetrahedra is another version of Marching Cubes, but they are separated into different sections for clear distinction and discussion between both algorithms.

2.4.1 Marching Cubes

The Marching Cubes algorithm was proposed by Lorensen and Cline (1987). The algorithm divided the 3D volumetric data into n number of cubes, and each cube represented a unit on isosurface. For every cube defined, the algorithm placed them between every two surfaces, as elucidated in the 3D volumetric data.

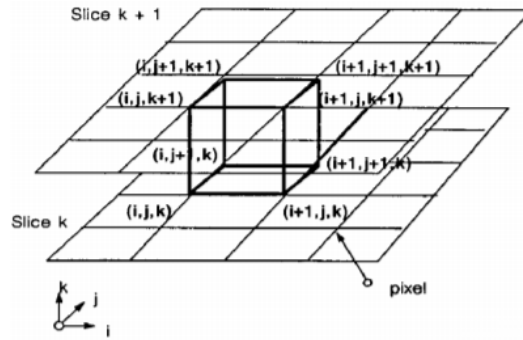


Figure 2.3 Marching Cubes between two surfaces (Lorensen & Cline, 1987)

As shown in Figure 2.3, the algorithm started with a defined cube placed between two surfaces. The vertices were labelled as such: if the vertex fell within the contour, it was labelled as 1, else it was labelled as 0. The cube's index was calculated based on the labelling in each vertex. The index was then compared with a lookup table of 256 cube configurations to get the equivalent cube configurations based on the index. The cube configurations can be categorized into 15 unique patterns, as shown in Figure 2.4, with the black dots representing vertices falling within the contour, as identified by Lorensen and Cline (1987). The result of the comparison was a list of edges. During triangulation, triangles were formed whereby each of its vertex was the midpoint of the returned edges (Lorensen & Cline, 1987). The algorithm then “marched” on to the next cube after successfully identifying the triangle vertices of the current cube.

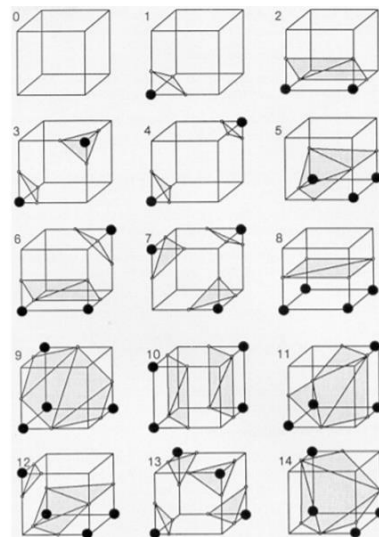


Figure 2.4 15 unique patterns of cube triangulation (Lorensen & Cline, 1987)

However, if the cube configurations followed the 15 unique patterns identified by Lorensen and Cline (1987), there would be ambiguity issues during the triangulation step. For example, take cube configuration number 6 followed by 12 from Figure 2.4. When placed side-by-side, a “hole” would appear in the middle during the triangulation step, as shown in Figure 2.5. The “hole” typically occurred when one of the cube’s vertices was positive, meaning within the contour, whereas its opposing cube’s matching vertex was negative, meaning not within the contour. This would become an issue in the reconstructed model as it may cause the model to have multiple “holes” on the surface. Most of the “hole” issues could be solved by defining all 256 cube configurations instead of condensing them into 15 unique ones.

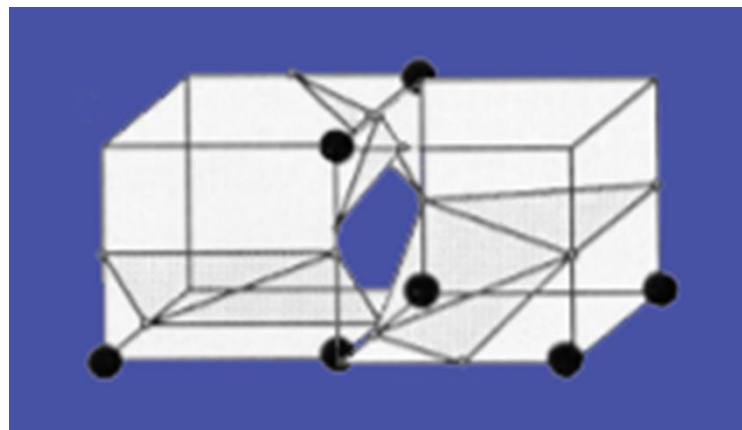


Figure 2.5 Marching Cubes ambiguity issue

Advantages of the traditional Marching Cubes algorithm include having the possibility to speed up the reconstruction process as the cubes were processed independently of one another; hence they could be processed in parallel, which may shorten the overall reconstruction time. Disadvantages of the Marching Cubes algorithm include slow reconstruction time depending on the input 3D volumetric data size as the number of cubes defined scales with the 3D data, a massive number of vertices and faces due to oversampling, resulting in a vast number of possible triangular patches that ultimately leads to bigger 3D model size, and ambiguity issue may still occur in certain cube configuration combinations caused by cube configuration

topology even when all 256 possible cube configurations were defined in the lookup table.

Even though the traditional Marching Cubes algorithm was founded in 1987, some recent publications still use it for reconstruction. For example, the 15 cube configurations of the Marching Cubes algorithm were used to construct polyhedral element meshes (Kim et al., 2019). The traditional Marching Cubes algorithm was also used for lumbar intervertebral disk herniation diagnosis (Al-Mnayyis et al., 2020).

Over the years, many improvement variations of the Marching Cubes algorithm were discovered and proven to perform better than the traditional one. For example, J. Y. Wang et al. (2020) proposed an improved Marching Cubes method that uses Laplacian smoothing to eliminate zero probability during isosurface extraction, and edge collapse method and polygon merging method to improve the display and interaction speed (J. Y. Wang et al., 2020).

After pre-processing the CBCT images, the 3D volumetric data was subjected to Laplacian smoothing during isosurface extraction process. All the retrieved vertices were smoothed through Laplacian smoothing to ensure that the probability of any vertex that does not appear in the retrieved vertices list is not 0 (J. Y. Wang et al., 2020). The smoothing process helped eliminate noise from the data, smooth out the isosurface, and fix most of the surface “hole” issues (J. Y. Wang et al., 2020). After the smoothing process, an edge collapse method was applied to reduce the number of vertices. The edge collapse method applied here was a surface simplification process using Quadric Error Metric (Garland & Heckbert, 1997). After applying the edge collapse method, the last step before the reconstruction ended was applying polygon normal regression, a polygon merging method (J. Y. Wang et al., 2020). The polygon merging method was applied to improve the contour, which suggests that the edge collapse, to a certain

extent, distorted the 3D model, requiring further processing to improve the surface of the 3D models. After defining an optimal merge threshold, the triangular patch geometric data was merged while complying with the threshold (J. Y. Wang et al., 2020).

One advantage of this improved Marching Cubes method was that the number of vertices and faces was significantly reduced, resulting in nearly half of the original models. Besides that, the reconstruction time was reduced considerably as well. However, because the CBCT dataset involved consists of only 320 and 512 image slices, the resolution for individual image slices was not stated. Also, there was no mention of whether the reconstruction accuracy was affected using the improved Marching Cubes method.

Another improved Marching Cubes algorithm involved redefining all the 15 unique cube topology configurations into 33 cube configurations, called Marching Cubes 33, which covered most of the complex trilinear function of topology cases, which addresses not just the ambiguity on the surface but also ambiguity within the cube itself (Chernyaev, 1995). The 33 cube configurations were as shown in Figure 2.6. Custodio et al. (2019) extended this work by grouping all 33 cube configurations into three categories during triangulation: simple leaves, tunnel, and interior point leaves (Custodio et al., 2019). Their work used the mentioned three triangulation groupings to perform Marching Cubes 33 extended triangulation to support all the complex cases of cube topologies in trilinear interpolation. The groupings were based on the final shape of the isosurface in the cube after deformation. If the deformed isosurface resembled a disc without requiring an additional point to support the representation, it was grouped into simple leaves triangulation (Custodio et al., 2019). If the deformed isosurface resembled a cylinder, it was grouped into tunnel

triangulation. In contrast, it was grouped into interior point leaves triangulation if the isosurface resembled a disc and required an additional vertex in the cube's center to support correct representation (Custodio et al., 2019). After all the connectivity between vertices was verified and all the cubes were grouped into any of the three categories, the triangulation was performed following each category triangulation rules and process.

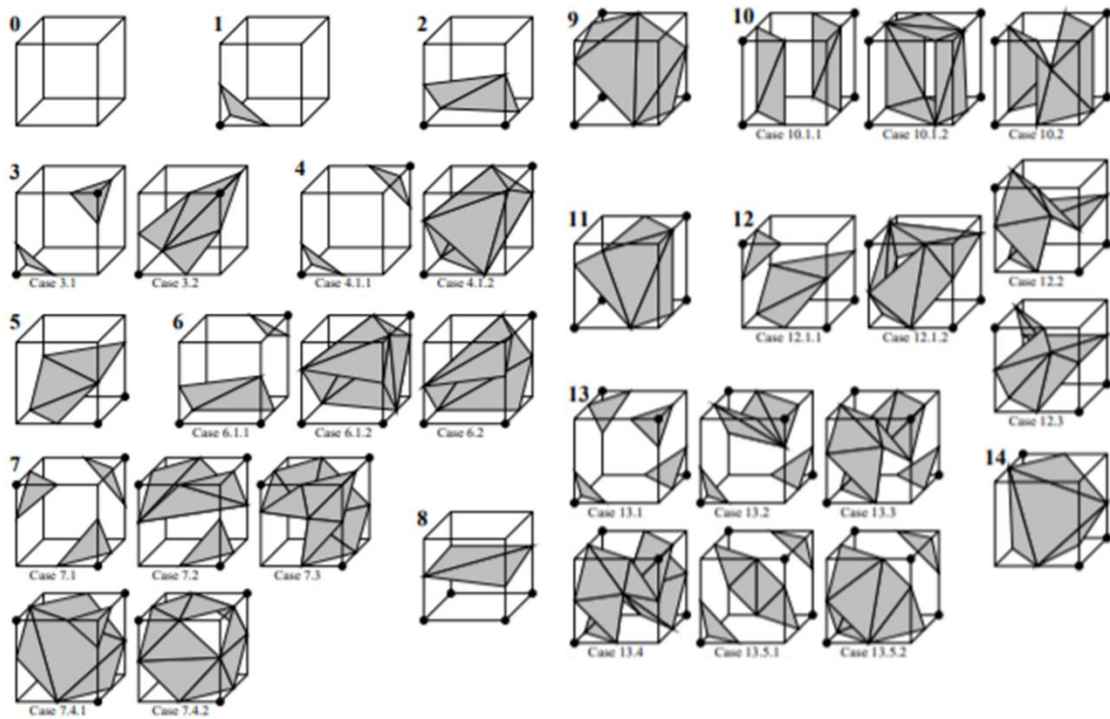


Figure 2.6 33 cube configurations (Custodio et al., 2019)

The advantages of this algorithm include improved triangulation quality in the reconstructed 3D models and solving the ambiguity issue in complex cube configuration cases (Custodio et al., 2019). However, the datasets used for testing were small. Secondly, there was no mention of whether the total execution time is affected.

An improvised Marching Cubes method was also applied to display a smooth 3D spine model, as mentioned by Wi et al. (2020). Like the method proposed by J. Y. Wang et al. (2020), they first apply Laplacian smoothing on the reconstructed surface using the Marching Cubes algorithm (Wi et al., 2020). It was to smooth out the rough

mesh surface, a common issue for 3D models reconstructed using the Marching Cubes algorithm. After smoothing out the surface using the Laplacian smoothing method, a mesh simplification algorithm was applied to reduce the number of triangular patches (Wi et al., 2020). The applied mesh simplification algorithm was the same as used in the improved Marching Cubes method proposed by J. Y. Wang et al. (2020), a mesh simplification method based on Quadric Error Metrics (Garland & Heckbert, 1997). After the mesh simplification step, they applied Taubin smoothing to prevent mesh shrinkage (Wi et al., 2020). This means that the 3D model will be potentially deformed if Taubin smoothing is not applied after simplifying the mesh, which affirms the downside of using mesh simplification methods.

Advantages of this method include the ability to support high-resolution CT images, lower processing time, and better quality of reconstructed 3D models (Wi et al., 2020). The disadvantage of this method was higher memory usage, which suggests that higher-end spec computers or workstations were needed for the reconstruction step. Also, there was no mention of the size of the image datasets used.

The improved Marching Cubes algorithm proposed by Purnama et al. (2020) was a simple and straightforward improvement involving extending the original 15 cubes configuration lookup table. The improved Marching Cubes algorithm was an adapted version proposed by Masala et al. (2013), which follows through similar processing steps taken in the traditional Marching Cubes algorithm, with the main difference being the extension on the lookup table from 15 unique cube topology configurations to 21 cube topology configurations (Masala et al., 2013). The 21 cube configurations were as shown in Figure 2.7.

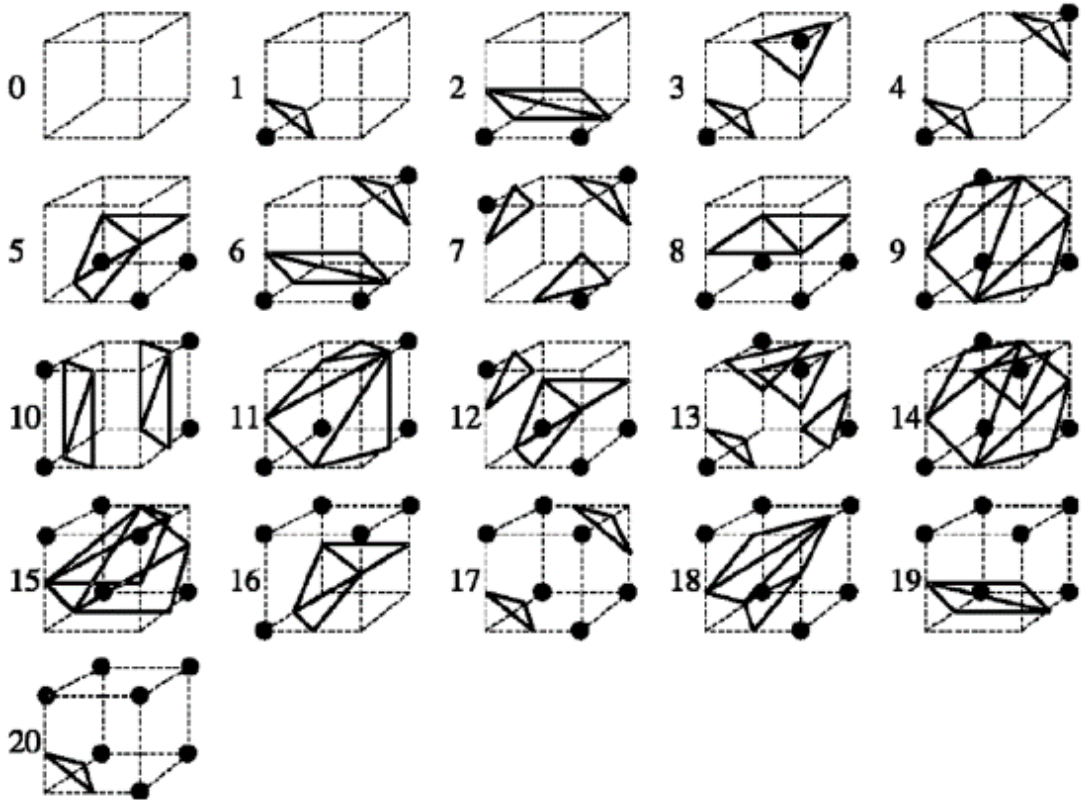


Figure 2.7 21 cube configurations (Masala et al., 2013)

The advantage of this improved algorithm was that the ambiguity issue in the traditional Marching Cubes algorithm was solved in most of the combined cube configuration cases with considerable performance (Purnama et al., 2020). However, the testing dataset only consisted of 161 and 162 image slices. Also, there was no mention of whether the number of triangular patches was affected.

Another improved Marching Cubes algorithm that involves expanding the 15 unique cube configuration lookup table was proposed by M. N. Wang (2020). Like the improved Marching Cubes algorithm proposed by Masala et al. (2013), they expanded the lookup table to 24 unique cube configurations (M. N. Wang et al., 2020). The 24 unique cube configurations were as shown in Figure 2.8. This further eliminated “holes” on the reconstructed surfaces, reducing ambiguity. Besides that, the reconstruction speed was also decreased by introducing multi-threaded parallel processing and a protocol mapping table. After dividing the 24 cube configurations into three unique